Temporal Fluctuations in a 100-A LaB_6 Hollow Cathode

IEPC-2013-385

Presented at the 33rd International Electric Propulsion Conference,
The George Washington University, Washington, D.C., USA
October 6–10, 2013

Benjamin A. Jorns* and Ioannis G. Mikellides† and Dan M. Goebel ‡
Jet Propulsion Laboratory, California Institute of Technology, Pasadena, CA 91109, USA

The temporal fluctuations in the near plume of a 100-A LaB_6 hollow cathode are experimentally investigated. At high currents, turbulent oscillations may contribute to two of the anomalous processes of hollow cathode operation—anomalous resistivity and the production of energetic ions. A detailed study of the properties of the oscillations in a high current cathode is necessary to determine the impact of the fluctuation spectrum on these two effects. In this investigation, a probe array is employed to measure the amplitude and dispersion of axial modes in the plume while a retarding potential analyzer yields estimates of the radial ion energy distribution. The onset of the ion acoustic turbulence is observed at high current values, and the character of the turbulent spectrum is shown to agree with weak turbulent theory: the amplitude of the spectrum decreases with flow rate but increases with discharge current. Estimates of the anomalous collision frequency based on experimental observations indicate that the IAT collision frequency can exceed the classical collision frequency at sufficiently high discharge current densities. Additionally, the onset of the IAT is shown to be correlated with the appearance of a high energy ion tail and that the energy in this tail is comparable to the energy in the experimentally-observed IAT.

*Associate Engineer, Electric Propulsion Group, benjamin.a.jorns@jpl.nasa.gov
†Principal Engineer, Electric Propulsion Group
‡Senior Research Scientist, Thermal and Propulsion Engineering Section

I. Introduction

Despite the fact that the hollow cathode (HC) is a staple of many of the electric propulsion systems flown today, there are two major physical mechanisms governing the behavior of these flight-critical elements that remain unclear. The first is the presence of anomalous resistivity in the cathode plume.[1] Without a knowledge of this effect, simulations of HC must be informed by experimental measurements. This dependence limits the ability of HC models to examine new design iterations and curtails their predictive capability for long life behavior. The second anomalous effect is the production of ions in the cathode plumes with energy significantly in excess of the discharge voltage. These high energy ions have been shown to be capable of completely eroding away the cathode keeper face[2,3] leading to a result which would be a significant failure mechanism any electric propulsion system that employs a hollow cathode

To date, our lack of understanding of HC physical processes has not prevented the successful qualification and implementation of deep-space missions that rely on this technology;[4–7] however, in light of new NASA programs that are calling for higher power EP missions with extended lifetimes, it is becoming increasingly important to resolve the unknowns in high-current HC operation. For example, a recent proposal of the NASA In-Space Propulsion Project, Game Changing Development (GCD) Program has called for 50-200 A cathodes with life capability that greatly exceeds 15,000 h. However, in the only extended lifetime study of a high-current hollow cathode performed to date, the keeper completely eroded within 8000 hours at 100 A.[8] In light of this limited performance, the need is apparent to design more durable cathodes. This can only be enabled through a more complete understanding of the cathode's anomalous processes.

With this in mind, a number of investigations have focused on identifying the nature of the high energy ions in high-current cathodes[9–17] Yet, while most of the proposed mechanisms have been applied with different degrees of success toward reproducing the erosion profiles of the life-tested NSTAR discharge hollow cathode, none of these previous investigations have addressed the issue of anomalous resistivity. On the other hand, a promising yet relatively unexplored contributor to this second effect is the onset of ion acoustic turbulence in the HC plume. This is a particularly promising candidate for explaining this effect in light of the nearly fifty years of experimental and theoretical work that has shown current-carrying plasmas can give rise to the IAT and that this instability can contribute significantly to enhanced effective collisonality.[18–20] Indeed, Mikellides et al demonstrated through a series of experimentally-informed models that the conditions in the HC plasma are suitable for the onset of the IAT.[1] These authors also found that the theoretical formulation of this instability has the correct dependence on plasma parameters to explain the anomalous resistivity that occurs in the hollow cathode plume. However, while this work was successful in capturing a number of the experimentally observed trends, the authors noted that that there was no experimental confirmation of the IAT. To be sure, acoustic modes have been proposed to explain some of the salient trends in the observed frequency spectra of probes inserted in the HC plume[21,22] but the acoustic nature of these waves has never been directly measured in the IAT.

As an additional consideration, even though the IAT has not been experimentally observed in the HC plasma, previous investigations have ruled out the iAT as a contributor to the production of energetic ions in favor of other processes.[9,15] This was justified based on the observation that high frequency fluctuations in the cathode plume where $\sim 10\%$ of the plasma potential and therefore could not explain ion energetic significantly above the discharge potential. However, these studies failed to estimate the total energy in the IAT, which due to the energy carried by the wave as it propagates through the plasma can can be substantially higher than the amplitude of the the potential fluctuation. The IAT therefore may still be a reasonable candidate for the onset of energetic ions.

In light of these considerations, a number of questions arise about the role of the IAT in the hollow cathode plume: does the IAT exist in the plasma plume? Does it result in anomalous collision frequency? If yes, does the collisionality correspond to the trends employed in previous simulations to correctly capture cathode behavior? And if the waves exist, do they have sufficient energy to lead to ion heating? The goal of this paper is to examine these questions experimentally and analytically. To this end, this paper is organized in the following way. In the first section, we briefly review the theory of current-driven turbulence in an unmagnetized plasma. In the second second, we describe the experimental setup to probe for the presence of this turbulence and its effects in the hollow cathode plume. In the third section, we present the results of the experimental investigation and discuss them in the context of the theoretical work. In the fourth and final section, we discuss the implications of IAT on hollow cathode performance.

II. Ion Acoustic Turbulence Theory

The ion acoustic (IA) instability is an electrostatic mode that naturally arises in plasmas where there is a large disparity in ion and electron temperatures $T_e/T_i \gg 1$ and where there is a significant electron drift velocity V_e. As such, hollow cathode plasmas with their strong electron current and low ion temperature are a prime environment for the onset of IA. In this section, we review the dispersion relation for this instability and we examine the impact the instability has on steady-state plasma parameters.

A. Linear Dispersion Relation

The collisionless processes that lead to the growth of the IA are inherently kinetic. We therefore examine the dispersion relation for the IA from a kinetic formulation. Implicit in the following derivation is that the plasma is uniform as compared to the wavelength $\lambda \ll L$ where L denotes the characteristic gradient length and that the wave vector k is in the same direction as the electron drift V_e. While this second assumption be violated for large amplitude waves (c.f. Refs. 18 and 23) where loss processes lead to a saturation of modes in the parallel direction, we assume saturation is sufficiently weak at the onset of the instability that propagation is primarily in the direction of the electron drift. With this in mind, allowing for weak collisionality, the dispersions relation for acoustic modes is given by[24]

$$k^2\varepsilon\left(\omega,k\right) = 0 = k^2 - \frac{1}{2}\sum_{s=e,i}\frac{1}{\lambda_{d(s)}^2}\frac{Z_0'\left(\zeta^{(s)}\right)}{1-2i\left(\nu_{(s)}/kv_{(e)}\right)Z_0\left(\zeta^{(s)}\right)}, \tag{1}$$

where ε denotes the dielectric tensor, $\lambda_{d(s)} = \frac{q^2 n_s}{\epsilon_0 T_s}$ is the Debye length of the s species and $Z_0\left(\zeta^{(s)}\right)$ is the plasma dispersion function:

$$Z\left(\zeta^s\right) = i\sqrt{\pi}e^{-\left(\zeta^s\right)^2}\left[1+\mathrm{erf}\left(i\zeta^s\right)\right] \tag{2}$$

$$\zeta^s = \frac{\omega + i\nu_s - kV_s}{k}\left(\frac{m_s}{2T_s}\right)^{1/2}. \tag{3}$$

Here ω is the wave frequency, k is the component of the wave vector parallel to the electron drift velocity, V_s is the drifting speed of the s species in the parallel direction, and ν_s denotes the collision frequency of the s species.

We consider the following ordering that is characteristic of the IA instability as well as the cathode plasma $v_i \ll c_s \ll V_e \ll v_e$ where $v_{i,e}$ denote the thermal speeds of the ions and electrons. In this limit, it is only necessary to consider the cases where $\left|\zeta^e\right| \ll 1$ and $\left|\zeta^i\right| \gg 1$. This allow us to simplify Eq. 1 considerably

$$k^2\varepsilon = 0 = k^2 - \omega_{pi}^2\left[-\frac{m_i}{T_e} + \frac{3T_i}{m_i}\frac{k^4}{(\omega')^4} + \frac{k^2}{(\omega')^2}\right] \tag{4}$$

$$-i\left[-\frac{\omega'/k - V_e'}{\lambda_{de}^2 v_e}\left(\left(\frac{\pi}{2}\right)^{1/2} + \left(\frac{\pi}{2}-1\right)\frac{\nu_e}{kv_e}\right) - \omega_{pi}^2\left(\frac{\nu_i}{\omega'}\left(\frac{k}{\omega'}\right)^2 + \left(\frac{\pi}{2}\right)^{1/2}\left(\frac{m_i}{T_i}\right)^{3/2}\frac{\omega'}{k}e^{-m_i\left(\omega'/k\right)^2/(2T_i)}\right)\right], \tag{5}$$

where we have transformed to the ion rest frame, $\omega' = \omega - kV_i$. The solution of this equation for the frequency as a function of the wavenumber yields the dispersion of the acoustic mode. Finding the exact dependence is difficult, however, in light of the equation's nonlinearity. Instead, we approximate the frequency dependence (c.f. Ref. 25, Chapter 4) by separating the dielectric tensor into its real and imaginary components: $\varepsilon\left(\omega,k\right) = \varepsilon_r + i\varepsilon_i$. Then, letting k be real, allowing $\omega' = \omega_r + \omega_i i$, and assuming a small growth rate, $\omega_i \ll \omega$, we can Taylor expand the dielectric function with respect to ω_r. This yields two equations

$$0 = \varepsilon_r\left(\omega_r,k\right) \tag{6}$$

$$\omega_i = -\frac{\varepsilon_i\left(\omega_r,k\right)}{\partial\varepsilon_r\left(\omega_r\right)/\partial\omega}.$$

Applying the first of these approximations to Eq. 5 yields

$$\left(\omega_r'\right)^2 = k^2c_s^2\left(\frac{1}{\left(\lambda_{de}k\right)^2+1} + 3\frac{T_i}{T_e}\right). \tag{7}$$

This is the kinetic dispersion for the real frequency of the IA mode. We note that in the cold ion case $T_i \to 0$, this dispersion exhibits a resonance at the plasma frequency $\omega = \omega_{pi}$, and, even allowing for finite ion temperature, this dispersion exhibits a significant change in character near the plasma frequency ω_{pi}. Finally, recalling that $\omega' = \omega - kV_i$, we find that in the laboratory frame the frequency is given by

$$\omega = k\left[c_s\left[(\lambda_{de}k)^2 + 1\right]^{-1/2} + V_i\right] \tag{8}$$

From Eq. 5 and the second line of Eq. 7, the imaginary part of the frequency is

$$\omega_i = \frac{1}{2}c_s k\left[\left(\frac{V_e' - c_s}{v_e}\right)\left[\left(\frac{\pi}{2}\right)^{1/2} + \left(\frac{\pi}{2} - 1\right)\frac{\nu_e}{kv_e}\right] - \left(\frac{\pi}{2}\right)^{1/2}\left(\frac{T_e}{T_e}\right)^{3/2} e^{-T_e/2T_i}\right] - \frac{1}{2}\nu_i, \tag{9}$$

where we have made the simplification $\omega'/k \approx c_s$ in order to arrive at this compact form. In this expression, the first term stems from electron Landau damping, the second is from electron collisional damping, the third term represents ion Landau damping, and the fourth term is from collisional damping due to ions. Following Ref.,[24] we note that subject to the conditions for the development of IA, we have $v_e\left(\nu_e/k\right) \approx \left(\nu_e/\omega\right)\left(m_e/m_i\right)^{1/2} \ll 1$. We therefore can neglect the second term in the growth rate as compared to the role of electron Landau damping. This yields the simplified form

$$\gamma = 2\omega_i = c_s k\left[\left(\frac{V_e' - c_s}{v_e}\right)\left[\left(\frac{\pi}{2}\right)^{1/2}\right] - \left(\frac{\pi}{2}\right)^{1/2}\left(\frac{T_e}{T_i}\right)^{3/2} e^{-T_e/2T_i}\right] - \nu_i, \tag{10}$$

where γ denotes the growth rate of the instability. The reason from this nomenclature stems from the fact that when $\gamma > 0$, the instability grows.

The kinetic interpretation of the first term in this result can be understood in the context of inverse Landau damping. The linear wave-particle interaction is localized to the particles with velocities close to the phase velocity of the propagating mode. The effect of this particle interaction is an irreversible process leading to the redistribution of particle energy in the vicinity of the phase velocity–a flattening of the velocity distribution. If there are more particles with velocities slightly below the wave phase velocity, i.e. the particle velocity distribution has a negative slope, the net effect will be a redistribution of energy to higher values at the expense of wave energy. On the other hand, if there are more particles with a velocity slightly above the wave phase velocity (a positive slope in the particle velocity distribution), the wave will gain energy at the expense of the particle energy. For a Maxwellian distribution, it is necessary for the drift velocity to exceed the wave phase velocity in order for this second process to occur. This condition on drift velocity translates directly to $V_e' > c_s$ for the ion acoustic instability, and in the limit of a collisionless plasma with $T_e \gg T_i$, this criterion similarly corresponds to the necessary and sufficient condition for the onset of the instability ($\gamma > 0$).[23,26]

The second term of Eq. 10 stems from Ion Landau damping and represents a sink on wave energy. It is dominant when $T_e \approx T_i$, and it is for this reason that that ion acoustic waves typically are only unstable in low temperature plasmas where thermal equilibrium has not been achieved between the two particle species. There is no mechanism for inverse ion Landau damping in the IA case since this acoustic mode necessarily propagates in the rest frame of the ions. This term therefore is an unconditional sink. Significantly, we note that balancing the growth rate of the IA against ion Landau damping can result in the growth of significant high energy ion tails. This has been observed in a number of experimental setups.[19]

The third term in Eq. 10 includes the effects of ion-species collisions. In the weakly ionized regime of the cathode plasma, we anticipate these collisions to be dominated by ion-neutral instances. This collisional sink in this case represents the dissipation of the wave by collisions of the ions that carry the mode with background neutrals. With this in mind and in light of the assumption $T_e \gg T_i$ that is valid for the cathode plasma, we assume that the ion collisions represent a larger sink than ion Landau damping. Subject to this assumption then, Eq. 10 simplifies to

$$\gamma = \omega'\left[\left(\frac{\pi}{2}\right)^{1/2}\left(\frac{V_e'}{v_e}\right) - \frac{\nu_i}{\omega'}\right], \tag{11}$$

which embodies the linear effects of the growth of the instability due to inverse electron Landau damping and its dissipation to collisions.

B. Turbulent Spectrum

While the linear theory from Eq. 11 indicates the criteria for when the ion acoustic instability can be driven unstable, it also suggests that for sufficiently large frequency, *any* ion acoustic mode can grow. This can give rise to a number of modes that propagate concurrently—the subsequent mixing of which leads to the formation of so-called ion acoustic turbulence (IAT). Ultimately, even though all of these modes can be excited, this amalgamation of propagating waves cannot grow indefinitely— some mechanism must arise for the turbulent spectrum to saturate. Linear theory does not provide a mechanism for this saturation, and as such, we are forced to include the dissipative effects of higher order kinetic effects in order to arrive at a steady state spectrum. To this end, we consider the kinetic equation for the steady-state power spectrum of the IAT first put forth by Kadmotsev[27]and modified to include ion-neutral collisions:[28]

$$0 = \left(\frac{\pi}{2}\right)^{1/2} \frac{V_e'}{v_e} - \frac{\nu_i}{kc_s} + \alpha \frac{T_i}{T_e} k\lambda_{de}^3 \frac{\partial \left[k^3 I_k\right]}{\partial k}, \tag{12}$$

where $I(k) = q^2[\phi(k)]^2/(T_e)^2/V_k$, V_k is a characteristic volume in wavenumber space and $\alpha = 32\pi(2/15)$. The first two terms contain the linear growth and dissipation while the second term contains both the effects of wave-wave coupling to lower frequency modes and nonlinear Landau damping.

Allowing the cutoff wavenumber to be $k = 1/\lambda_{de}$, we can integrate Eq. 12 to find the steady-state power spectrum:

$$I(k) = \alpha \left(\frac{T_e}{T_i}\right) \frac{1}{k^3} \left(\frac{V_e'}{v_e} \log\left[\frac{1}{\lambda_{de}k}\right] - \frac{\nu_i}{\omega_{pi}} \left(\frac{2}{\pi}\right)^{1/2} \left[\frac{1}{k\lambda_{de}} - 1\right]\right). \tag{13}$$

We in turn can convert this result to frequency space through the relation $I(k)V_k = I(\omega')V_{\omega'}$:

$$I(\omega') = \alpha \left(\frac{T_e}{T_i}\right) \frac{1}{(\omega')^3} \left(\frac{V_e'}{v_e} \log\left[\frac{\omega_{pi}}{\omega'}\right] - \frac{\nu_i}{\omega_{pi}} \left(\frac{2}{\pi}\right)^{1/2} \left[\frac{\omega_{pi}}{\omega'} - 1\right]\right). \tag{14}$$

This expression represents the steady-state IAT spectrum that results when the dominant processes in the plasma are inverse electron Landau damping for the growth of the wave and collisional and nonlinear processes for its dissipation. In the limit $\omega' \gg \nu_i$, this expression simplifies to

$$I(\omega') \propto \frac{1}{(\omega')^3} \log\left[\frac{\omega_{pi}}{\omega'}\right], \tag{15}$$

which is the so-called Kadmotsev spectrum[27] in frequency space. This result indicates that with increasing frequency the amplitude of the ion acoustic turbulence decreases. On the hand, from Eq. 14 we can see that at the low frequency end of the spectrum, ion collisions become dominant and prevent the growth of the wave. The spectrum therefore disappears at both extremes of frequency range, and as such, we can infer the existence of optimum. To determine where this peak is frequency space, we differentiate Eq. 14 with respect to frequency:

$$0 = -\omega' \frac{V_e'}{v_e} \left(1 + 3\log\left[\frac{\omega_{pi}}{\omega'}\right]\right) - \frac{\nu_i}{\omega_{pi}} \left(\frac{2}{\pi}\right)^{1/2} (3\omega' - 4\omega_{pi}). \tag{16}$$

Now, in the low frequency limit we have $\omega \ll \omega_{pi}$ such that Eq. 16 reduces to

$$\omega = 4\nu_i \left(\frac{2}{\pi}\right)^{1/2} \frac{v_e}{V_e'} \left(3\log\left[\frac{\omega_{pi}}{\omega'}\right]\right)^{-1} \left(1 + \frac{V_i}{c_s}\right). \tag{17}$$

$$\omega = 4\nu_i \left(\frac{2}{\pi}\frac{m_i}{m_e}\right)^{1/2} \frac{1}{V_e'} \left(3\log\left[\frac{\omega_{pi}}{\omega'}\right]\right)^{-1} v_\phi, \tag{18}$$

where $v_\phi = c_s + V_i$ denotes the laboratory phase velocity of the ion acoustic instability. We thus find that in the presence of weak collisionality, the maximum of the turbulent spectrum depends linearly on the ion collision frequency and the electron mach number. This result is physical intuitive as we anticipate the maximum should occur at the frequency where the collisional process becomes dominant over the nonlinear

effects, i.e. where $\omega \sim \nu_i$. In a weakly-ionized plasma, this correspondence suggests a scaling of the maximum frequency with neutral particle density ($\nu_i \propto n_n$) where n_n is the neutral density.

Finally, we can substitute Eq. 18 into Eq. 15 to find the scaling for the potential amplitude of the IAT spectrum:

$$\phi\left(k\right)^2 |_{max} \propto \frac{T_e}{T_i} \frac{\left(V_e'\right)^4}{\nu_i^3}. \tag{19}$$

By employing this result as a proxy for the magnitude of the IAT spectrum, we arrive at the physically intuitive conclusion that the IAT spectrum will be larger in amplitude for higher electron temperature and for larger drift velocities. The former dependence reflects the fact that in direct analogy to linear ion Landau damping for acoustic modes, the nonlinear ion processes for damping become less important for a higher ratio of electron to ion temperature. The second trend reflects the fact that the IAT is driven unstable by the relative electron drift. On the other hand, the inverse dependence of the amplitude on the collision frequency embodies the effect of ion neutral collisions on dissipating the IAT. Since the ion collision frequency is dependent on neutral density, this suggests the IAT may be damped at higher flow rates. We examine this possibility in the experimental section.

C. Anomalous Collision Frequency

As we have seen from Eq. 11 and Eq. 15, the main driver for positive growth of the IAT is inverse electron Landau damping. This suggests that the energy for the ion acoustic instability comes at the expense of electron velocity. Effectively, the electrons are slowed down to add energy to the propagating waves. This energy transfer is irreversible and consequently can be modeled by an effective collision frequency. To arrive at an expression for this effective term, we quote the result of weak turbulent theory:[23]

$$\nu_{AN} \approx \omega_{pe} \frac{W}{n_0 T_e}, \tag{20}$$

where ω_{pe} denotes the electron plasma frequency and W is the total energy density in the IAT given by

$$W = \frac{\varepsilon_0}{2} \int_0^{1/\lambda_{de}} \omega' \left[k\phi\left(k\right)\right]^2 \frac{\partial \epsilon_r}{\partial \omega'} dk, \tag{21}$$

where $\left[\phi\left(k\right)\right]^2$ in this case implicitly is a spectral density. From Eq. 20, Eq. 5, and allowing $\omega' = c_s k$, we thus find

$$\nu_{AN} = \frac{\omega_{pe}}{2} \int_0^{1/\lambda_{de}} \left[\phi\left(\omega\right)\right]^2 d\omega, \tag{22}$$

where we have made the conversion to frequency space. This is the classical representation of IAT anomalous resistivity, and we can see from this expression that the larger instability, the more energy it must extract from the electrons in order to be maintained.

D. Ion Heating

The onset of ion acoustic turbulence has long been associated causally with the heating of plasma ions and the formation of high energy tails.[19] The mechanisms by which the ion acoustic modes produce this heating can be grouped into three categories: ion Landau damping, nonlinear ion Landau damping, and wave dissipation through collisions. The first two processes are collisionless in that they exchange energy with the part of the ion velocity distribution that is resonant, i.e. close to the phase velocity of the wave or its nonlinear components. The third, collisional process, on the other hand, can heat ions outside the resonant conditions. This is because ion collisions serve to disrupt the coherent motion of the wave. In a collisionless environment, ion acoustic waves are carried by the oscillations of non-resonant ions in a completely reversible way. There is therefore no energy transfer to them. However, if the wave motion is interrupted by collisions, the process can become irreversible and characterized by a net transfer of energy to the non-resonant ions.[29]

The self consistent formulation for the transfer of energy to ions in a collisional plasma is an ongoing subject of discussion with a number of experiments, theoretical formulations, and numerical simulations. For

this investigation, in lieu of attempting to self-consistently evaluate the mechanism by which the energy is transferred to the ions, we instead follow the treatment of Ref. 29 by calculating the total energy carried by the ions in the ion acoustic waves. Assuming this energy can be transferred to the ion population through either tail formulation or bulk heating, this quantity thus serves as an upper bound for the amount of energy that the IAT can transmit to the ions.

With this in mind, we consider that that since the IAT is an acoustic mode, its energy is carried by the ions. The wave energy density for a single mode in the IAT is therefore given by[25]

$$\tilde{W}_i(k) = \frac{\varepsilon_0}{2} k^2 \phi(k)^2 \omega \frac{\partial \varepsilon_r}{\partial \omega}, \tag{23}$$

From Eq. 5, we can approximate $\partial\varepsilon_r/\partial\omega = 2\omega_{pi}^2/(\omega - kV_d)^3$. We thus find that

$$\tilde{W}_i(k) = n_0 \frac{q^2}{T_e}\left(1 + \frac{V_i}{c_s}\right)\phi(k)^2, \tag{24}$$

where we have made the substitution $\omega = k\left(1 + \frac{V_i}{c_s}\right)$. This expression represents the energy *density* carried by the ions in the wave. In order to find the average energy, we must divide by the density $\tilde{n}$ of ions carrying the mode:

$$\tilde{E}_i(k) = \frac{n_0}{\tilde{n}} \frac{q^2}{T_e}\left(1 + \frac{V_d}{c_s}\right)\phi(k)^2. \tag{25}$$

Now, for electrostatic modes, we can make the approximation

$$\phi = \frac{T_e}{q}\frac{\tilde{n}}{n_0}. \tag{26}$$

The average energy carried by the ions in the mode with wavenumber k therefore becomes

$$\tilde{E}_i(k) = q\left(1 + \frac{V_d}{c_s}\right)\phi(k). \tag{27}$$

For the case of $V_d \to 0$, this result is physically intuitive as it suggests the average energy in the electrostatic mode is the magnitude of its potential drop. However, we note that the IAT consists of a wide range of excited modes. To find the total energy in the turbulent spectrum then, we integrate with respect to wavenumber

$$E_t = q\left(1 + \frac{V_d}{c_s}\right)\int_0^{1/\lambda_{de}} \phi(k)\, dk, \tag{28}$$

where we implicitly have made the transformation of ϕ to units of spectral density. Converting to frequency space we find

$$E_T = q(c_s)^{-1}\left(1 + \frac{V_d}{c_s}\right)\int_0^{\omega_{pi}} \phi(\omega)\, d\omega. \tag{29}$$

This end result suggests that if the amplitude and width of the IAT spectrum in frequency space are large, the energy carried by the turbulence can be significantly larger than just the energy, $q\phi(\omega)$, of a single component of the spectrum.

Armed with this expression as well as the results of the scaling laws we found from the previous sections, we are now in a position to evaluate the properties and effects of any IAT that we may experimentally observe in our hollow cathode plume. With this in mind, in the following section we describe the experimental setup and diagnostics we employed to characterize propagating waves in the hollow cathode plume.

III. Experimental Setup

In this section, we describe the cathode we investigated as well as the diagnostics we employed to examine the development and impact of ion acoustic turbulence.

A. Cathode Assembly

The 100-A cathode assembly (Fig. 1) in our experiment was designed with the purpose of achieving high current output. As reported in detail in Ref. 30, it consists of a graphite tube that houses a LaB_6 insert. A tungsten endplate with an orifice that is 12% the diameter of the cathode tube caps the end. The cathode tube is wrapped with a tantalum coaxial heater that in turn is housed in a graphite keeper. The ratio of the keeper orifice to the keeper diameter is 15%.

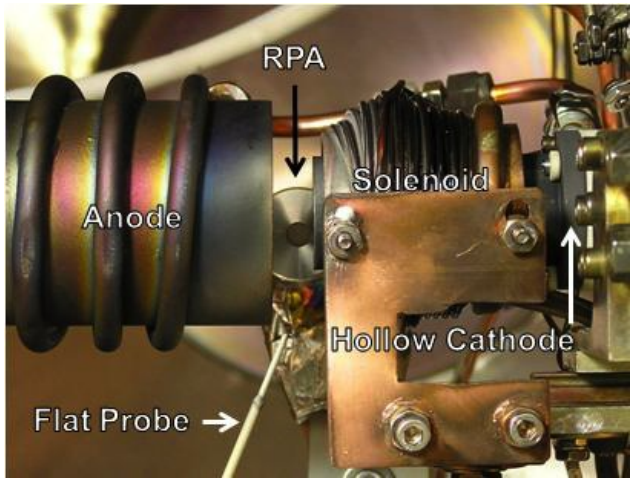

Figure 1. Photo of the 100 A hollow cathode employed in the experiment. The retarding potential analyzer and ion saturation probe array are also indicated.

The setup was installed in the JPL High Current Test Facility, a 2.8 m x 1.3 m cylindrical chamber with vacuum maintained by two cryopumps. The base pressure of this facility is $\sim 10^{-7}$ T while at the max flow condition examined of 20 sccm xenon, the background pressure was mainained at 3.7×10^{-4} T. A water-cooled, copper cylinder that was lined with tungsten served as the anode. This was placed ~ 3 cm downstream of the keeper face. While the cathode setup was surrounded by a solenoid capable of generating a magnetic field, for the measurements reported here, no magnetic field was applied.

B. Diagnostics

We performed three types of measurements during these trials: background plasma characterization, in situ plasma fluctuation measurements , and ion energy measurements. We discuss in the following the diagnostics we employed to perform these measurements and the analysis techniques we used.

1. Langmuir Probe

The background plasma density and temperature were measured with a single Langmuir probe located 0.75 cm downstream of the keeper face and placed on axis. The exposed element was 2 mm in length with a diameter of 0.5 mm. The reported electron temperature was inferred from an exponential fit to the probe IV trace (c.f. Ref. 31), while we employed the thin sheath approximation for cylindrical probes to estimate density, $n_i = i_{sat}/\left(0.61 q A_p \sqrt{T_e/m_i}\right)$ where A_p denotes the probe area. The measurements reported here were generated from an average of thirty-two probe traces.

2. Retarding Potential Analyzer

In order to characterize ion energy, we employed a four-grid, retarding potential analyzer (RPA). The first grid of the RPA was allowed to float while the second, electron repelling grid was biased negatively with respect to ground. The third and fourth grids were connected in parallel and provided the bias voltage necessary to resolve ion energies. The collector plate was grounded through a 1 MHz resistor, and we inferred the ion current from the drop across this resistor. We generated IV characteristics for this setup by sweeping the bias voltage from 0 to 100 V at 0.5 Hz and averaging over 16 traces.

The IV characteristics from the RPA yield information on the distribution of ion-to-charge energies in the plasma. In particular, we have[32]

$$-\frac{dI}{dV} = \beta \sum_s q_s^2 \eta_s f_i^{(s)} \left(q_s V\right), \tag{30}$$

where β is a constant, q_s denotes the charge of the s ion species (e.g. singly, double, triply charged), η_s is the fraction of the ion density comprised of the s species, and $f_i^{(s)}$ is the energy distribution of the s ion species. From this relation, it is evident that without a priori knowledge of the fraction of multiply charged states in the plasma, the interpretation of the IV characteristic is problematic. However, assuming the plasma is dominated by singly charge species, then this diagnostic is a proxy for ion energy

$$-\frac{dI}{dV} \approx \beta \sum_s q^2 f_i \left(q_s V\right). \tag{31}$$

3. Ion saturation probes

To characterize the on-axis, current-driven fluctuations in the cathode plume, we employed the dual ion saturation probe setup shown in Fig. 1. It consisted of two exposed tungsten tips oriented along the axial direction. The length of each tip was 2 mm and each probe was biased to -30 V with a battery. The purpose of this diagnostic was to measure fluctuations ion saturation current i_{sat} since these in turn serve as a proxy for plasma potential. In particular, as we indicated in the previous section, for electrostatic modes such as the ion acoustic wave, we have

$$\phi \approx \frac{T_e}{q} \frac{\tilde{n}}{n_0}. \tag{32}$$

The ion saturation current, however, is a direct proxy for density $i_{sat} = \alpha n_i$ where α is a constant dependent on electron temperature and probe dimensions. Assuming electron temperature fluctuations are small compared to density perturbations, we thus can see from Eq. 32 that

$$\phi = \frac{T_e}{q} \frac{\tilde{i}_{sat}}{\bar{i}_{sat}}, \tag{33}$$

where $\bar{i}_{sat}$ denotes the time averaged quantity. By measuring the fluctuations in ion saturation current then, we thus are able to infer fluctuations in potential.

Armed with this relation, we can characterize the nature waves in the plasma by correlating the signal between probe tips. The principle of this technique can be illustrated by representing the fluctuations in the plasma with an eikonal representation:

$$\phi = \sum_k \phi\left(\omega\right) e^{i\left(k(\omega)x - \omega t\right)}, \tag{34}$$

where $k\left(\omega\right)$ is the wavenumber at frequency ω and $\phi\left(\omega\right)$ denotes the complex amplitude of the wave with frequency ω. The fluctuation in potential as measured at two different positions in x is thus measured as

$$\phi_1\left(t\right) = \sum_\omega \phi_1\left(\omega\right) e^{i\left(k(\omega)x_1 - \omega_k t\right)} \tag{35}$$

$$\phi_2\left(t\right) = \sum_\omega \phi_2\left(\omega\right) e^{i\left(k(\omega)x_2 - \omega_k t\right)}. \tag{36}$$

The Fourier transform $\mathcal{F}$ with respect to time of these two signals yields

$$\mathcal{F}\left[\phi_1\left(t\right)\right] = \phi_1\left(\omega\right) e^{ik(\omega)x_1} \tag{37}$$

$$\mathcal{F}\left[\phi_2\left(t\right)\right] = \phi_2\left(\omega\right) e^{ik(\omega)x_2}. \tag{38}$$

From these quantities, we can see the relation

$$\mathcal{F}\left[\phi_2\left(t\right)\right] \mathcal{F}^*\left[\phi_1\left(t\right)\right] = \phi_1\left(\omega\right) \phi_2\left(\omega\right) e^{i\Delta x k(\omega)}. \tag{39}$$

And from this we find the wavenumber:

$$k(\omega) = \frac{1}{\Delta x} \tan^{-1} \left[\frac{\mathrm{Im}\left[\mathcal{F}\left[\phi_2(t)\right] \mathcal{F}^*\left[\phi_1(t)\right]\right]}{\mathrm{Re}\left[\mathcal{F}\left[\phi_2(t)\right] \mathcal{F}^*\left[\phi_1(t)\right]\right]} \right]. \tag{40}$$

In this way, we can find the distribution of wavenumber $k(\omega)$ along the vector between the two probe tips (axial in our case) where the range of discernible wavenumber is dictated by the separation between probes, $|k| < \pi/\Delta x$.

The accuracy of this approach can be improved in a noisy plasma by averaging over a number of time signals. However, if there are multiple modes present in the plasma, i.e. multiple wave numbers for a fixed frequency, this technique can be errant. In order to resolve the distribution of k at a fixed ω, we employ the histogram technique first proposed by Beall.[33] In particular, we perform a number M of time samples and evaluate the wavenumber as a function of frequency for each run according to Eq. 40. We then bin the k values and weight them according to

$$S(\omega, k) = \frac{1}{M} \sum_{j=1}^{M} I_{0,\Delta k}\left[k - k^j(\omega)\right] \frac{1}{2}\left[P_1^{(j)}(\omega) + P_2^{(j)}(\omega)\right]. \tag{41}$$

Here j indicates the run number, $P_1^{(j)}, P_2^{(j)}$, are the power spectra of the two signals, and we have defined the function

$$I_{0,\Delta k}(x) = \begin{cases} 1 & 0 < \Delta k \\ 0 & |x| > \Delta k \end{cases}$$

where Δk is the width of of the bin. Eq. 41 provides a means for us to visualize the dominant frequency and wave numbers in $k - \omega$ space. The subsequent results reported here consist of 100 averages with a resolution of $\Delta k = 0.83$ m^{-1} (for 150 bins) and a frequency resolution of $\Delta f = 10$ kHz.

IV. Results

In the following section, we present the results of a parametric investigation of the oscillations in the plume of the 100 A LaB_6 cathode. All measurements were performed on-axis at 0.75 cm from the keeper face. We examined operating conditions with four flow rates of xenon, 8 sccm, 10 sccm, 15 sccm, and 20 sccm over the discharge current range $I_D = 20$ A $-$ 130 A.

A. Background measurements

We show measurements of the plasma temperature and density in Fig. 2 as functions of increasing discharge current. At 8 sccm, the temperature strictly increases with discharge current, while at higher flow rates the electron temperature is non-monotonic—passing through a minimum value and then rising. Moreover, the overall magnitude of electron temperature decreases with flow rate. This latter trend is consistent with previous experiment investigations[30] and suggests that collisional damping leads to an overall depression in electron temperature. On the other hand, in direct contrast to our measurement of temperature in the cathode plume as a function of current, in Ref. 30 it was reported that *inside* the same cathode tube and at fixed flow rate, the electron temperature decreased monotonically with discharge current. This discrepancy between internal and external measurements may stem from the relationship between electron temperature and resistive heating in the plume. In particular, although the electron temperature decreases inside the cathode with increasing discharge current due to internal processes, at sufficiently high discharge currents, local effects in the plume—such as the onset of the IAT— may give rise to enhanced colllisionality in the plume. This in turn can lead to local heating subsequent increase in electron temperature. In this case, the initial decrease in temperature with current we observe in Fig. 2 would reflect the fact that at low currents, the resistive heating in the plume is sufficiently low that the plume temperature is a proxy for the the internal cathode processes (decreasing temperature with current). It is only when the resistive effects in the plasma become sufficiently high that the external resistivity becomes dominant and the temperature in the plume deviates from the experimentally observed trends inside the cathode.

In terms of plasma density, we find the physically intuitive result that the density increases monotonically with discharge current at all flow conditions. Moreover, at constant discharge current, the density is within a factor of two at all flow conditions.

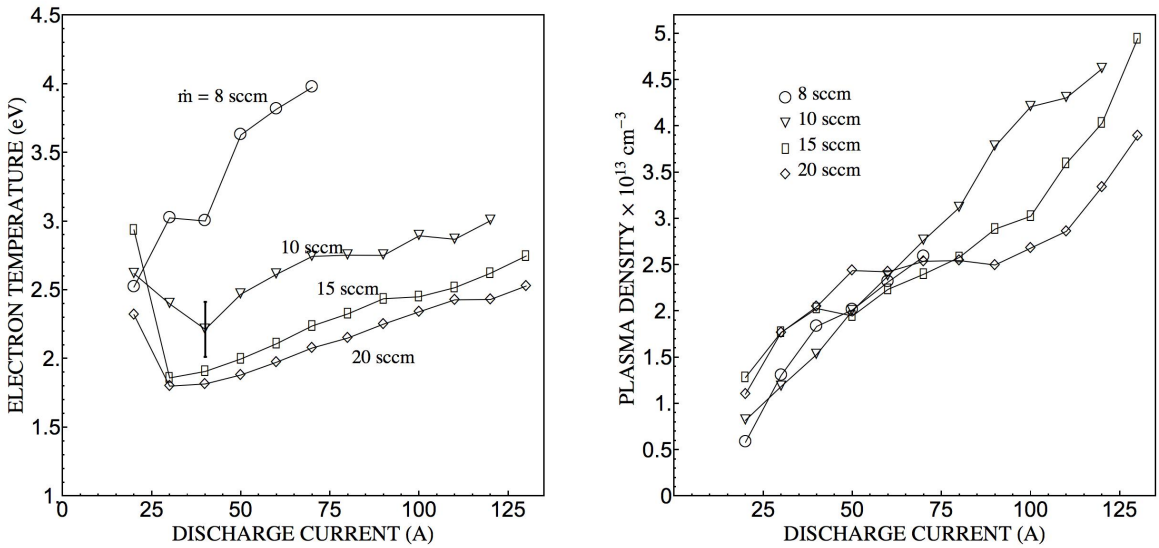

Figure 2. Electron temperature and density as functions of discharge current at four different flow rates. A representative error bar is shown for the temperature while the density is accurate to within 50%.

B. Dispersion relation

In Fig. 3, we show Beall intensity plots for three current conditions at the flow rate of 10 sccm. These two dimensional intensity plots reflect the dominant modes in frequency and axial direction at a position 0.75 cm from the keeper face and on the cathode axis. The top plots illustrate a larger frequency range at a resolution of 10 kHz while the lower plots were taken at a higher frequency resolution, 1 kHz, in order to resolve features in the low kilohertz frequency regime.

It is evident from these figures that with increasing discharge current, there is a shift in the character of the axial modes. In particular, at low discharge current, the intensity plots are dominated by a low frequency mode < 100 kHz with harmonics that appear at higher frequency values. Moreover, we can see from the $I_D = 30$ A case that the dispersion of this mode is nonlinear with an effective wavenumber that "zig-zags" with frequency. The change in sign with wavenumber suggests that this mode may be some type of standing wave in the plasma characterized by two counter-propagating waves. This idea is borne out by our observation that with increasing current ($I_D = 70$ A), the low frequency mode becomes effectively dispersionless, $k = 0$. Moreover, this low frequency mode is consistent with previous investigations of fluctuation spectra in hollow cathodes,[15,21,22] and the lack of coherent dispersion lends further support to the idea that these modes are ionization instabilities with a non-dispersive character.[15]

With increasing current, we can see from Fig. 3 that the low frequency instability is replaced by a high frequency mode with a clearly linear dispersion. This is illustrated by the the transition from the $I_D = 70$ A condition where the two modes coexist to the $I_D = 110$ A case where the high frequency mode is dominant with a maximum near 800 kHz. From both plots, we can see the high frequency mode is subject to phase wrapping. In other words, since the probe spacing is limited to a finite width Δx, modes with wavelengths shorter than the spacing between the probe tips appear as lower wavenumbers with $k = 2\pi\left(\lambda^{-1} - n/\Delta x\right)$ where $n = \lfloor \Delta x/\lambda \rfloor$. Given the linearity of the dispersion, however, we can adjust for this phase wrapping by translating the plot with respect to wavenumber as we have done in Fig. 4 to see the true dispersion of the mode.

We note that while we have only shown the representative case of $\dot{m} = 10$ sccm here, we have observed this transition of the low frequency mode giving way to the higher frequency mode with increasing current at all of the flow conditions except for 20 sccm. In this case, all frequency content was muted and we did not see the emergence of the IAT. On the the other hand, while the transition between modes did exist for the flow rate $\dot{m} = 15$ sccm, we found the interesting result that the high frequency mode disappeared for intermediate currents only to return at low values ($I_D < 40$ A).

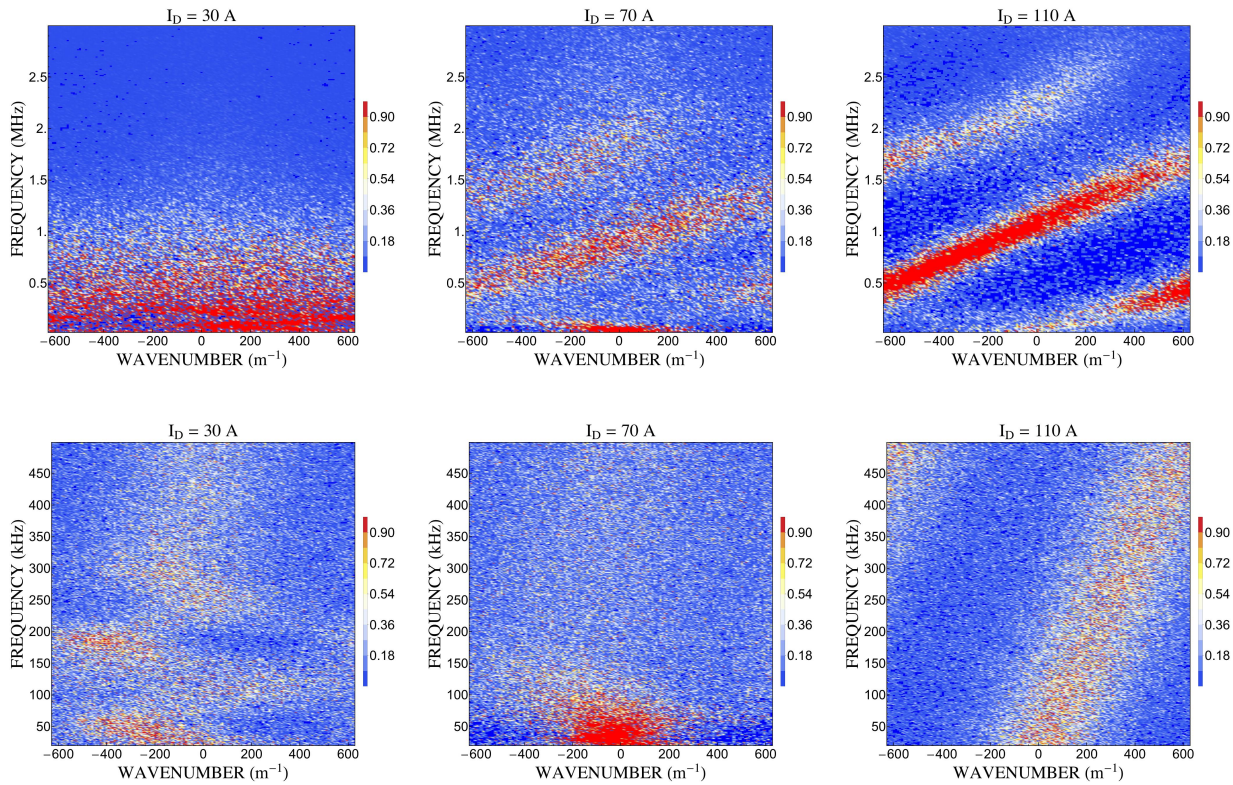

Figure 3. Beall plots with increasing current for the axial wavenumber at the flow condition $\dot{m} = 10$ sccm. Each plot is normalized to its maximum. The frequency resolution on the top plot is 10 kHz while the resolution on the bottom plot is 1 kHz.

The linear nature of the high frequency mode in the direction of electron drift indicates that it is the ion acoustic instability ($\omega \propto k$). As further evidence of this, we have fit a line to the dispersion plot for all of the flow conditions where we could resolve the acoustic instability above the background. An example of such a fit is illustrated by the dotted line in Fig. 4, and the results of these fits over the investigated parameter space is shown in Fig. 5. We also show the calculated sound speed $c_s = \sqrt{T_e/m_i}$ for the same conditions. It is evident from these plots that the measured phase velocity tracks the ion sound speed, although there is an offset in all cases of ~ 3 km/s. This discrepancy can be explained by the fact that while the acoustic instability propagates with the sound speed in the ion rest frame, Eq. 8 shows that in the laboratory frame, the phase velocity of the wave is the sum of the ion sound speed and the ion drift velocity. Our measured results therefore suggest an axial ion drift of the ions of ~ 3 km/s. This is consistent with previous laser induced fluorescence measurements of ion velocities in a hollow cathode[34] as well as the simulations of our 100 A LaB_6 high current cathode.[35]

The linear dispersion of the axial wavenumber coupled with its proximity to the acoustic speed both lend support to the conclusion that the observed mode is the ion acoustic instability. Moreover, as we can seen from Fig. 3, the ion acoustic spectra generally is dominant for $k > 500$ m^{-1}, which is an observation we found to be consistent over the operating conditions where we could resolve the IAT. Given the characteristic axial length scale of the plume in our experiment was ~ 10 cm, the short wavelength of the IAT ($\lambda < 1$ cm) in the axial direction suggests that the results from the kinetic formalism of Sec. II that are valid for a locally uniform plasma can be applied. In light of this assumption, we now can investigate additional details into the the nature of the experimentally-observed IAT and compare these results directly with the the kinetic formalism from Sec. II. With this in mind, in the following section we examine the power spectra as a function of flow rate and discharge current.

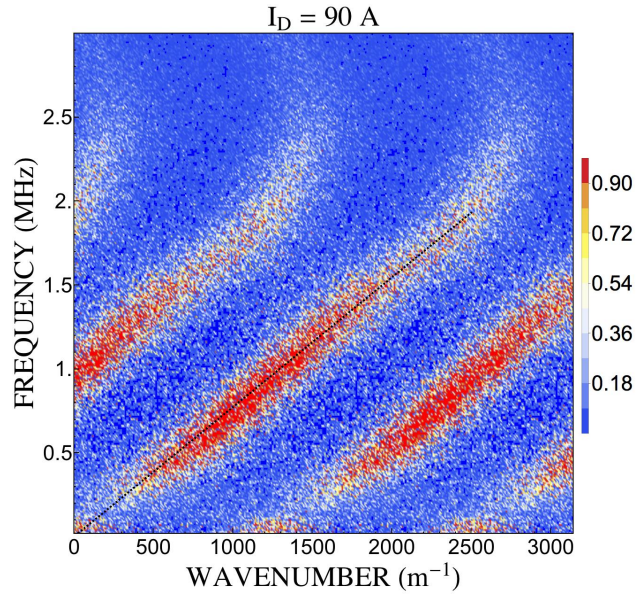

Figure 4. The intensity plot when phase-wrapping is corrected for the case of $I_D = 90$ A and $\dot{m} = 10$ sccm. The dotted line is a best fit to the linear dispersion of the acoustic mode.

C. Power spectra

In order to determine the impact of discharge current on the axially-propagating modes in the cathode plume, we show in Fig. 6 power spectra measured by the on axis ion saturation probe at the operating condition of $\dot{m} = 10$ sccms. The two disparate modes discussed in the previous section are apparent in these plots: the low frequency < 100 kHz peak and the high frequency peak that appears with increasing current. While these figures do not provide the same information about dispersion as the Beall plots from the previous section, they can help better illustrate the frequency trends of the two modes. In particular, we can see that the location of the low frequency peak as well as its amplitude decrease with increasing discharge current. On the other hand, the high frequency, ion acoustic instability grows in amplitude and maintains an approximately constant frequency at its maximum value. The first of these trends— the growth of the ion acoustic turbulence with discharge current— is consistent with our theoretical results from in Sec. II.B where we found that the magnitude of the ion acoustic should increase with electron temperature and drift velocity. In particular, while our measurements of increasing density with discharge current in Fig. 2 suggests that the electron drift velocity may be approximately constant ($V_e' \propto n_e/I_D$), the electron temperature does increase with discharge current.

From Fig. 6, we also see that it is possible to compare directly the amplitude of the two modes. As we can see from the left hand side, the IAT begins to emerge at $I_D = 40 - 50$ A. However, from the right hand plot, it is apparent that by $I_D = 90$ A the two modes have comparable amplitudes, and ultimately, at $I_D = 110$ A, the higher frequency mode is dominant. The peak at this high current condition is two orders of magnitude lower than the peak exhibited by the peak of the lower frequency mode at $I_D = 20$ A. This does not necessarily suggest, however, that the energy in the low frequency mode is higher. The total energy is dictated by the sum of all of the frequency components (Eq. 29), and as can be clearly seen, the width of the low frequency peak at $I_D = 20$ A is significantly narrower than the spectrum exhibited by the IAT instability at $I_D = 110$ A.

In order to determine the impact of flow rates, we show in Fig. 7 the power spectra at fixed current for four flow conditions. Two salient trends emerge from these results: the impact of flow rate on the magnitude of the oscillation spectrum and the dependence of the location of the IAT's peak on flow rate. For the former trend, we note that at high frequencies, the magnitude of the power spectrum decreases with increasing flow. Since the neutral density is linear with flow rate while we have found the plasma density remains approximately constant (Fig. 2), this result suggests that ion-neutral collisions plays a role in damping the high frequency, ion acoustic mode. The same decrease in amplitude with flow can be observed for the low frequency mode with the notable exception at $I_D = 20 - 30$ A, where the $\dot{m} = 8$ sccm case exhibits a lower

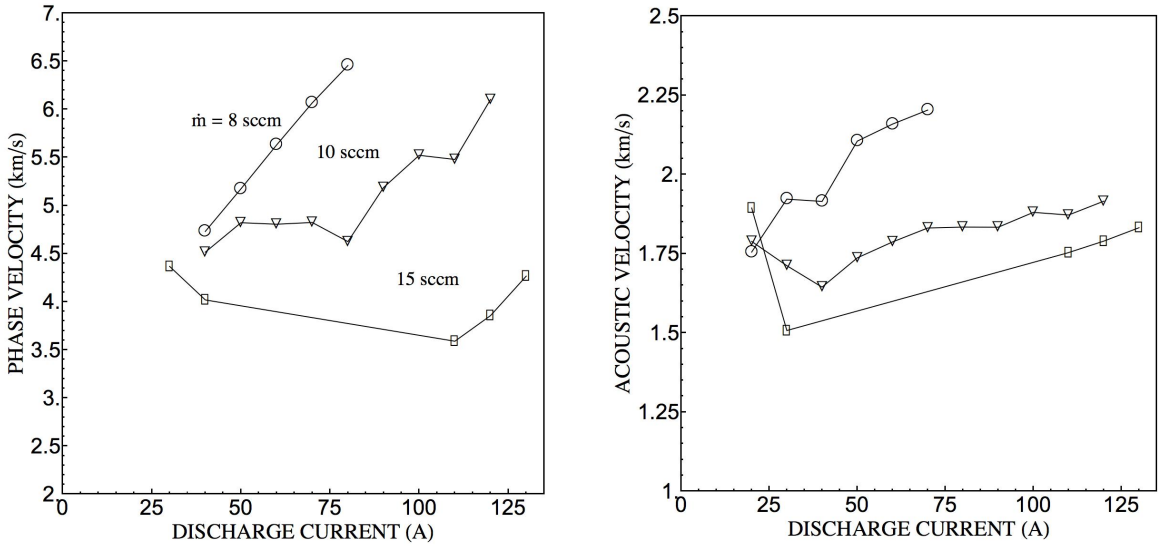

Figure 5. Left: Phase velocity of the acoustic mode as a function of discharge current at different mass flow rates. The IAT could not be resolved at $\dot{m} = 20$ sccm. The absence of points in the $\dot{m} = 15$ sccm reflects our inability to detect the dispersion of the mode in this range. Right: the calculated sound speed c_s at the same conditions.

overall spectrum than the $\dot{m} = 10$ sccm case. As for the latter trend of the location of the IAT's frequency peak, we can see from the $I_D = 80, 100, 110$ A cases that while the the maximum of the spectra does not change significantly with discharge current for a fixed flow rate, it does increase with flow rate.

These two trends with flow rate—damping of the waves and movement of the frequency peak—support the conclusions of Sec. II.B where we found that the frequency of the maximum should be dependent on neutral density and that the amplitude is inversely dependent on the neutral density (ion collision frequency). Moreover, our observation of the dependence of the IAT amplitude on the discharge current appears to be consistent with the results from kinetic formalism where we found the amplitude should depend on electron temperature. With the purpose of more precisely examining the agreement of all of these qualitative trends with the theory, we in the following sections tempt to quantify the observed power spectrum trends and compare the results to the theoretical work from Sec. II.

D. Kadmotsev Spectrum

In order to begin to relate the results from the previous section to the kinetic formalism from Sec. II, it first is necessary to test the key assumption of this work: the ion acoustic turbulence is saturated by nonlinear ion processes. To this end, we consider the trends from Figs. 6 and 7 where it is evident that once the IAT has onset, the frequency spectra experiences a nonlinear decay. As we discussed in Sec.II B this decay may be due to nonlinear wave-wave and wave-particle processes that transfer energy from higher frequency ion acoustic modes to the lower frequencies, and if this is the case, the fall off the the spectra should be characterized by a ω^{-3} dependence (Eq 15). To examine this possibility, we show in Fig. 8 a sample log-log plot of the power spectrum of the IAT where we have fit a line to the characteristic fall off of the spectrum with frequency.

The slope of the fitted line is -2.8, which corresponds to a decrease in power spectrum amplitude of $\omega^{-2.8}$. This close proximity to theory suggests that the Kadmotsev spectrum and its nonlinear decay is the dominant process for the depicted case in our low temperature plasma— a result consistent with other investigations of low temperature plasmas.[36] Following this log-log plotting technique, we have examined the decay of the power spectra for all of the flow rate conditions and discharge current values where we could identify from the Beall plot technique that the ion acoustic mode was present. The results of this parametric investigation are shown on the right side of Fig. 8 along with the theoretical value of the Kadmotsev spectrum.

The good agreement with theory over a range of flow conditions and currents lends further support to the

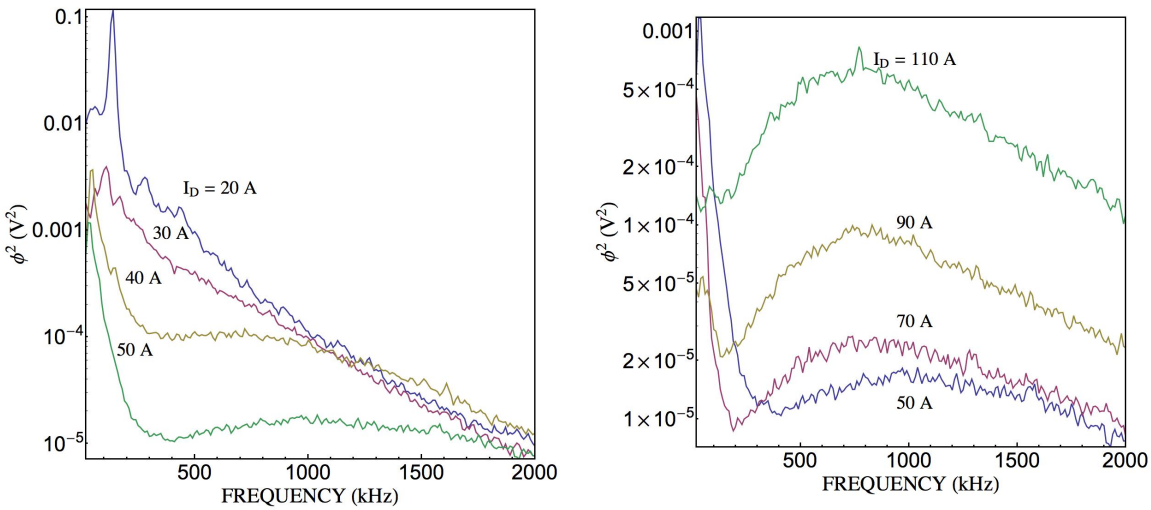

Figure 6. Power spectra for $\dot{m} = 10$ sccm as a function of increasing current. The left hand diagram illustrates the low frequency mode's behavior as it disappears with increasing current. The right hand plot shows the growth of IAT with increasing current. Note, the two plots are on different axes.

notion that the turbulence is dominated at higher frequencies by the the nonlinear processes associated with the Kadmotsev spectrum. We thus can be confident in the assumptions inherent to the theory we employed in Sec. II to arrive at a steady-state shape of the ion acoustic power spectrum, and in turn, we are free to interpret our experimental results— most notably the dependence of the peak on plasma parameters—in the context of this theoretical spectrum.

E. Location of the peak

In Fig. 9, we show the frequency values where it was possible to identify a maximum of the IAT. A peak did not exist at all operating conditions as the lower frequency mode was dominant or the IAT had not onset above the noise. However, when a peak did occur, as we can see from Fig. 9, the value did not depend significantly on discharge current. This is consistent with the theoretical results from Eq. 18: assuming the ion collision term is approximately constant for a given a flow rate, the frequency at the peak should depend linearly on the IAT phase velocity. As we can see from Fig. 5, the change in phase velocity at a fixed flow rate is less than 15% over the range where we could observe a max. The frequency at the peak therefore—just as we observe—should not change with discharge current. On the other hand, we can see from Fig. 9 that the magnitude of the frequency at the peak is monotonically dependent on flow rate. Assuming the ion collision frequency is monotonically related to neutral density, this trend with flow rate supports the observation from Sec. II.B where we found the location of the maximum should depend linearly on ion collisionality. We note the significant caveat, however, that even though the decrease in frequency follows from our expressions in Sec. II.B, without a direct measurement of neutral density or electron drift, we cannot directly examine the exact dependence of the form of our expressions from this section.

Regardless, the experimental trend of peak frequency coupled with our observation that the frequency decays in the Kadmotsev sense serves to support the conclusion that the IAT is dominated by nonlinear wave-wave and wave-wave-particle damping at the high frequencies while at the lower end of the spectrum, ion collisionality damps the mode. The interplay between the two processes leads to the optimum value we have observed.

F. Collision frequency

For the flow rates and discharge currents where we observed the IAT, we show in Fig. 10 the collision frequency based on our measurements of the power spectrum and Eq. 22. The IAT was never sufficiently

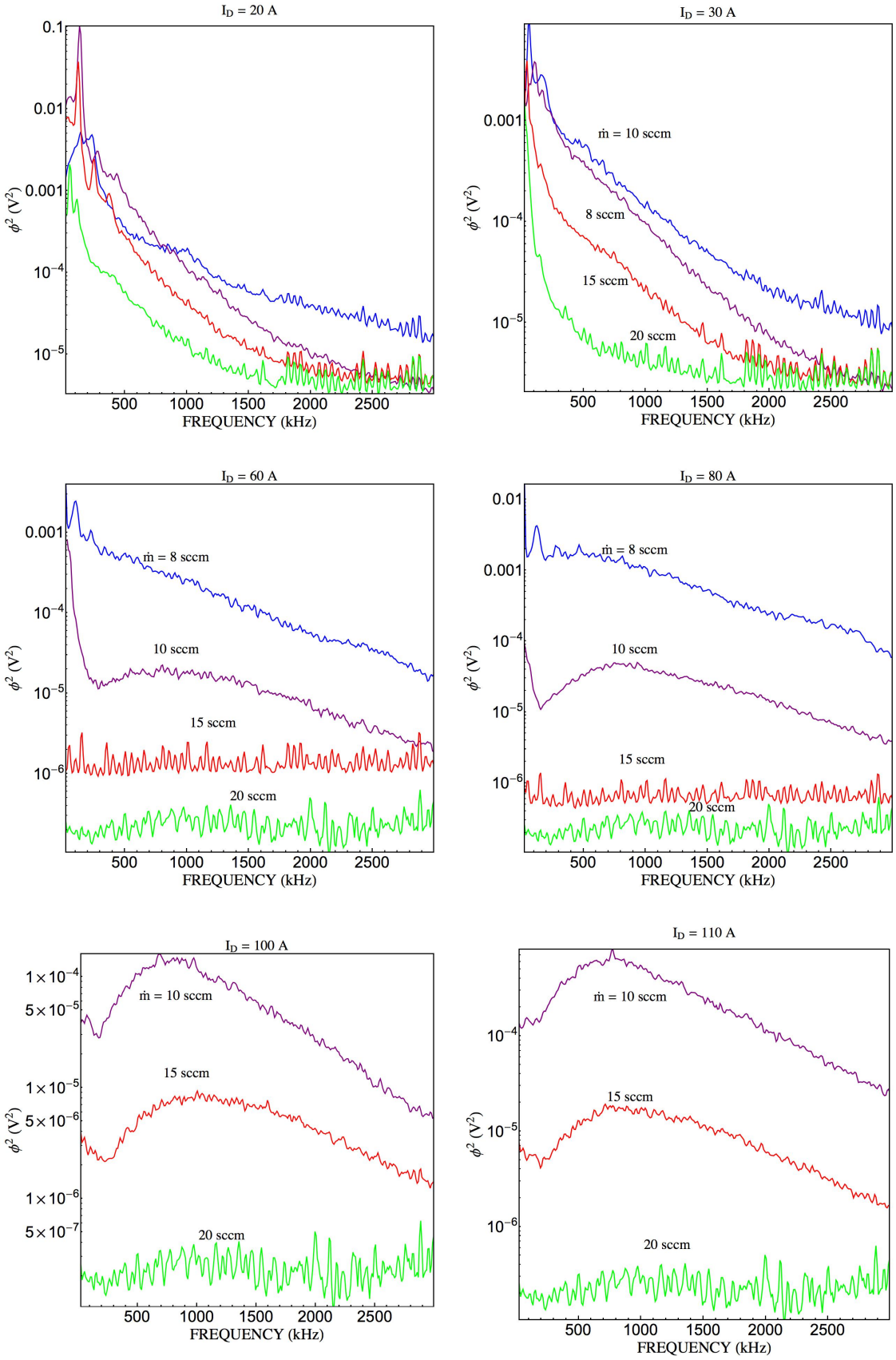

Figure 7. Log plots of power spectra for fixed currents and different flow rate.

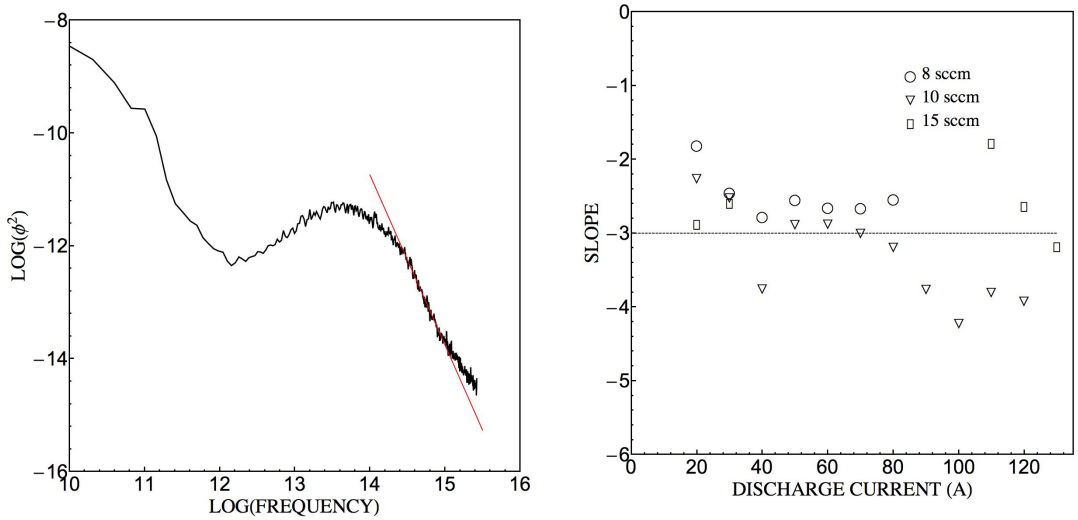

Figure 8. Anomalous resistivity as a function of discharge current. The indicated plots correspond to the conditions where the dispersion of the IAT could be confirmed from the dispersion plots.

above noise in the 20 sccm case to resolve the collisionality; however, it is apparent from this plot that for the cases when we could estimate the collision frequency, it exhibited the same increasing trend with discharge current for all flow rates. This stems directly from the increase in amplitude in the IAT with discharge current showcased in Fig. 6. Additionally, we can see from Fig. 10 that the amplitude of the collision frequency drops by an order of magnitude between flow rates. This trend reflects the damping of the turbulent spectrum with increasing flow rate we observed in Fig. 7.

In a companion paper,[35] simulations of the 100 A cathode at the axial position where our measurements were performed have shown that the necessary anomalous collision frequency to model the measured plasma parameters for a flow rate of 12 sccm is on the order of 10^8 s^{-1}. Extrapolating based on our results from Fig. 10 suggests that our result closely approaches this frequency. This agreement lends support to the conclusion that the anomalous resistivity invoked in this model is IAT driven.

In order to estimate the relative importance of the IAT collision frequency in driving the plasma parameters, we show on the right hand side of Fig. 10 the classic electron-ion collision frequency based on our measurements of the local plasma parameters:

$$\nu_{ei} = 2.9 \times 10^{-12} n_0 T_e^{-3/2} \left[23 - 0.5 \log \left(\frac{10^{-6} n_0}{T_e^3} \right) \right], \tag{42}$$

where n_0 is the background density in units of m^{-3}. It is evident from this result that the anomalous collision frequency does not always exceed the classical term. Rather, it is only for sufficiently high current densities (as embodied by $I_D/\dot{m}$) that we see the anomalous resistivity becomes dominant. This is a significant consideration for modeling the plume of high current cathodes as it suggests that it may not always be necessary to invoke anomalous effects.

As a final note, we return to our discussion from Sec. III.A where we pointed out that the growth of this anomalous collision frequency may explain the increase in electron temperature with discharge current exhibited in Fig. 2. Enhanced collisionality can lead to electron heating, which in turn would be reflected by a local increase in electron temperature. The same trends exhibited by the collisionality and electron temperature supports this thesis.

G. Ion energy

As a final check of the effects of the IAT, we examine the ion energy as a function of discharge current at the flow rate where anomalous collisionality (and therefore the anticipated ion heating) was the largest: 8 sccm. For this case, we show the normalized RPA traces as well as the inferred ion energy distributions (assuming

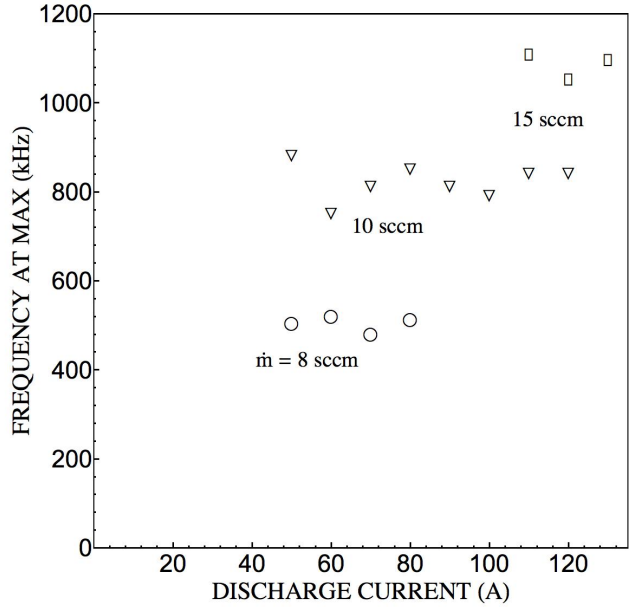

Figure 9. Frequency values at the maximum of the IAT power spectra where a peak could be identified and the dispersion plots revealed an acoustic mode. While there were peaks for the $\dot{m} = 20$ scam case at a higher frequency value, the dispersion of the IAT could not be confirmed.

dominant single charge states) as functions of increasing current in Fig. 11. Each energy distribution plot exhibits a peak in the $15-20$ V range. This is a characteristic energy on the order of the discharge voltage that reflects the energy gained by ions as they fall through the steady-state potential of the plasma. These peaks are consistent with previous radial RPA measurements of the ion energy distribution in hollow cathodes.[15] With increasing discharge current, however, we note a high energy ion tails begins to develop in the higher energy range $50 - 80$ V. This development is also consistent with previous investigations of unmagnetized hollow cathode plumes where it was noted that since the energy in the tail greatly exceeds the most probable value, there must be an acceleration mechanism beyond from the steady-state potential drop that leads to this high energy ion energy production.[9]

As we discussed in Sec. II.D, the IAT provides a mechanism by which a high energy ion tail can form. However, in order to establish this possibility as a viable mechanism, we need to determine if the IAT has sufficient energy to explain the increase in energy. To this end, we have employed Eq. 29 and our measurements of the power spectral density to estimate the average energy carried by the waves. This quantity is plotted in Fig. 12 as a function of discharge current. This figure indicates that the energy in the IAT is comparable to the tail energy, which in turn suggests that this process may be a sufficient mechanism to explain the onset of this high energy tail.

This result is a significant departure from previous discussions of the IAT in the hollow cathode plume, where this process was ruled out as a possible heating source for the ions.[9,15] These conclusions were based, however, on the assumption that the energy gained from propagating modes is the amplitude of the largest potential oscillation in the high frequency spectrum. The IAT, however, consists of several modes that are excited concurrently and that all carry energy. Given the wide frequency range of the IAT that we have observed, however, it is unsurprising that the total energy in this spectrum can greatly exceed the potential drop of just one of the constituent modes.

V. Discussion

From the above results, we now can draw a few conclusions about the impact of the IAT on the hollow cathode plume and discuss these conclusions in light of ongoing and future investigations of the two anomalous effects in the hollow cathode—the high resistivity and the anomalous ion energies.

With respect to the anomalous resistivity, we can itemize the following conclusions about the IAT spec-

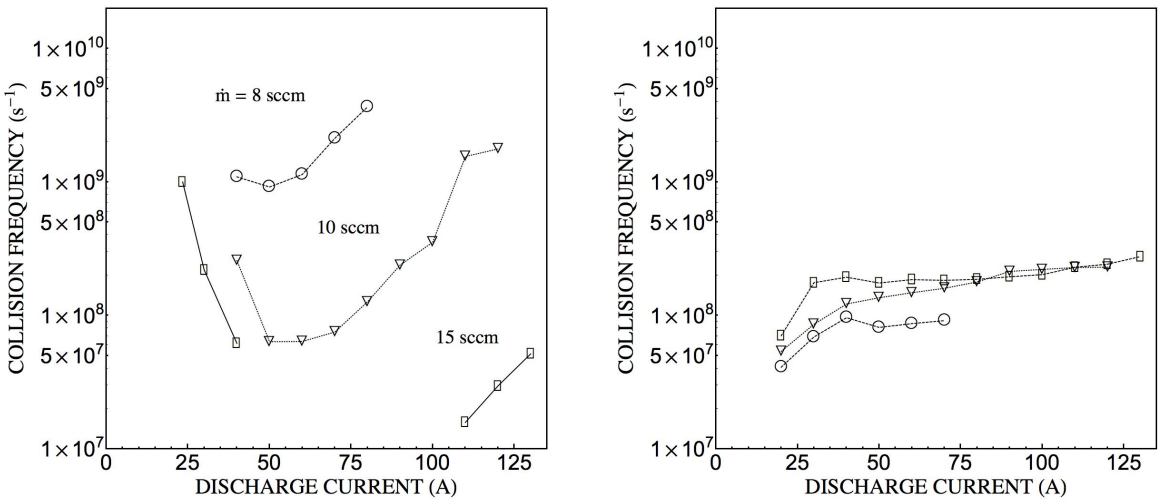

Figure 10. Left: effective collision frequency due to the IAT. Right: the classical electron-ion collision frequency based on measurements of the electron temperature and density.

trum:

1. The IAT exists in the hollow cathode plume as evidenced by the clear ion acoustic dispersion.
2. The IAT spectrum has a Katmodsev-like decay at high frequencies.
3. The experimentally measured anomalous collision frequency exceeds classical frequencies for high current densities.
4. The experimentally-observed anomalous collision frequency closely matches the value required to successfully capture the plasma parameters in a simulation of the 100 A cathode.

Taken together, these observations provide experimental proof for the first time that the use of anomalous collisionality is justified in simulations of the hollow cathode plume. Moreover, the agreement of results with the predictions from turbulent kinetic theory confirms the validity in the choose of the form for anomalous collisionality that has been successful in previous hollow cathode codes in capturing experimentally observed steady-state parameters. The correspondence between theory, simulation, and experiment all suggest then that we have successfully identified the major contributor to anomalous resistivity in the hollow cathode plume.

In terms of ion energy, we have showed theoretically and experimentally how there is a process for IAT to transfer energy to the ions: the waves are driven unstable at the expense of energy in the electron drift. The waves in turn transfer energy to the ions through collisional and resonant processes. Our analysis has shown that it is not appropriate to ignore this IAT-driven process as a possible mechanism for ion energy transfer as there is sufficient energy in the IAT to describe the formation of the anomalous ion energy tail. While ultimately we cannot rule out other proposed processes for the production of the high energy ions, previous experimental work does lend support to the idea that the IAT transfers energy to the ions. In particular, Chu and Goebel found that introducing additional flow into the cathode plume greatly reduced the production of energetic ions in the same 100 A we cathode we investigated. While they contended this effect was due to a damping of the low frequency, very coherent and large amplitude ionization modes, the same argument can apply to the damping of the IAT. In particular, from our theoretical work in Sec. II and our experimental results Sec.III C, we have direct evidence for how the amplitude of the IAT is extremely susceptible to extreme damping in the presence of increased flow rate. This could explain the observed reduction in energetic ions reported in these findings.

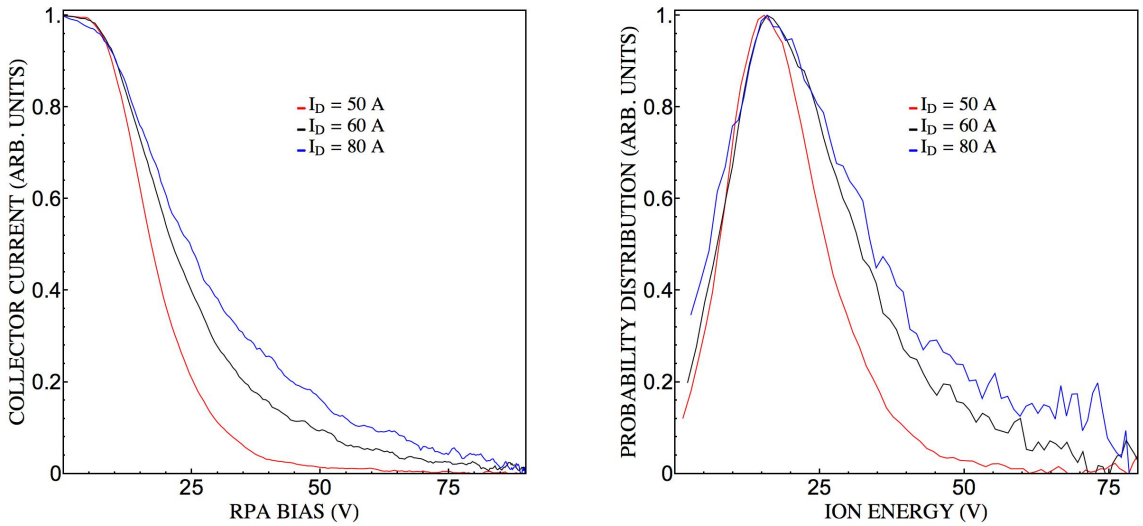

Figure 11. Left: ion collector current as a function of RPA bias voltage for $\dot{m} = 8$ sccm. Three cases for discharge current are shown, and all traces have been normalized to their maximum value. Right: the probability distribution of the ion energy subject to the assumption of singly charged ions.

VI. Conclusion

In this work, we have presented a parametric investigation of ion acoustic turbulence in the plume of a 100 A LaB_6 cathode. We have reviewed the theory for how IAT can lead to the onset of anomalous resistivity at the expense of the current in the hollow cathode discharge and how the growth of this instability can in turn lead to the production of a hig energy ion tail. Through a series of probe diagnostics, we have implemented an experimental setup in which we were able to successfully detect the onset, growth, and ultimate dominance of the IAT at high discharge. We furthermore have investigated the details of the power spectra exhibited by these waves over a wide range of discharge current and flow rate. Our findings match the predictions of turbulent kinetic theory, and this correspondence suggests the following mechanism for IAT onset: while the IAT is driven unstable by electron drift, nonlinear processes lead to a redistribution of the wave energy from high frequencies to low values while ion collisional damping leads to cutoff of the wave at low frequencies.

We have demonstrated how the agreement between the kinetic theory and our experimental observations lends support to the use of anomalous collisionality in models of the hollow cathode, and through direct measurement, we have confirmed that anomalous resistivity is present and dominant at high discharge currents in the hollow cathode. This collision frequency is within an order of magnitude of the value employed in a companion paper to model successfully the LaB_6 cathode at 100 A.

Finally, we have examined the energy carried by the IAT and compared it with the onset of a high energy tail as measured by a radially located RPA. Our analysis has shown that there is sufficient energy in the waves to explain the onset of high energy ions, which in turn suggests that the IAT cannot be dismissed as a candidate for anomalous energetic ion prediction in the hollow cathode. We further have discussed experimentally and theoretically how energetic ion production can be reduced through increased collisionality and how this idea is supported by experimental results reported outside this investigation which showed that higher neutral flow rates can reduce the energetic ion population.

In sum, the goal of this work has been directed toward exploring the role of the IAT in contributing the anomalous processes of high current hollow cathode. In identifying the IAT as a significant contributor to anomalous resistivity in the hollow cathode plume, we believe the results of this work can be used to help inform future models for hollow cathode performance. Similarly, through the identification of the IAT as another possible mechanism for energetic ion production, our knowledge of its growth and damping may provide a means for mitigating the effects of energetic ions. These two results may be significant mission

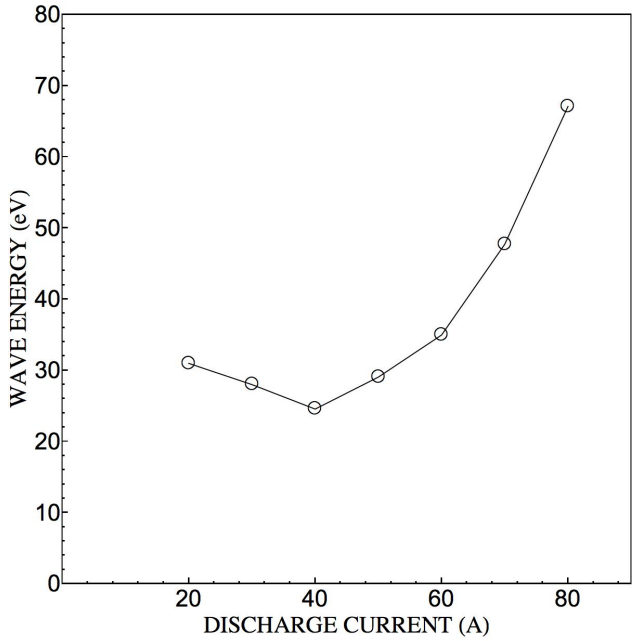

Figure 12. The total energy in the IAT for the $\dot{m} = 8$ sccm case as calculated from Eq. 29 as a function of increasing discharge current.

enablers as the need for higher current hollow cathodes is realized.

Acknowledgments

The research described in this paper was carried out by the Jet Propulsion Laboratory, California Institute of Technology, under a contract with the National Aeronautics and Space Administration and funded through the internal Research and Technology Development program.

References

[1]Mikellides, I. G., Katz, I., Goebel, D. M., and Jameson, K. K., "Evidence of nonclassical plasma transport in hollow cathodes for electric propulsion," *Journal of Applied Physics*, Vol. 101, No. 6, 2007, pp. 063301.

[2]Polk, J., Anderson, J., Brophy, J., Rawlin, V., Patterson, M., Sovey, J., and Hamley, J., "An overview of the results from an 8200 hour wear test of the NSTAR ion thruster," *AIAA Paper, 99-2446. June, 1999*.

[3]Sengupta, A., Brophy, J. R., and Goodfellow, K. D., "Status of the extended life test of the Deep Space 1 flight spare ion engine after 30,352 hours of operatio," *AIAA Paper, 03-4558. July, 2003*.

[4]Rayman, M. D., "The Successful Conclusion of the Deep Space 1 Mission: Important Results without a Flashy Title," *IAF abstracts, 34th COSPAR Scientific Assembly*, Jan. 2002.

[5]Koppel, C., Marchandise, F., Prioul, M., Estublier, D., and Darnon, F., "The SMART-1 Electric Propulsion Subsystem around the Moon: In Flight Experience," *41st Joint Propulsion Conference and Exhibit, Tucson,AZ, 10-13 July 2005. AIAA 2005-3671.*, 2005.

[6]Garner, C., Brophy, J., Mikes, S., and Rayman, M., "In-Flight Operation of the Dawn Ion Propulsion System- The First Nine Months," *44th AIAA/ASME/SAE/ASEE Joint Propulsion Conference, 20-23 July, 2008, Hartford, CT. AIAA-2008-4917*, 2008.

[7]Brophy, J. R., Polk, J. E., Randolph, T. M., and Dankanich, J. W., "Lifetime Qualification of Electric Thrusters for Deep-Space Missions," *44th Joint Propulsion Conference, AIAA-2008-5184, Hartford, CT*, 2008.

[8]Brophy, J. and Garner, C., "Tests of High-Current Cathodes for Ion Engines," *AIAA/ASME/SAE/ASEE 24th Joint Propulsion Conference,Boston, MA*, No. AIAA Paper 88-2193, 1988.

[9]Friedly, V. and Wilbur, P., "High current hollow cathode phenomena," *Journal of Propulsion and Power*, Vol. 8, No. 3, 2008, pp. 635–643.

[10]Kameyama, I., "Effects of Neutral Density on Energetic Ions Produced Near High-Current Hollow Cathodes,," Tech. Rep. NASA CR-204154, Oct. 1997.

[11]Williams, G., Domonkos, M. T., and Chavez, J. M., "Measurement of doubly charged ions in ion thruster plumes," *27th International Electric Propulsion Conference, Pasadena, CA, IEPC-01-310*, 2001, pp. 15–19.

[12]Katz, I., Mikellides, I. G., Goebel, D. M., Jameson, K. K., and Johnson, L., "Production of high energy ions near an ion thruster discharge hollow cathode," *42nd AIAA/ASME/SAE/ASEE Joint Propulsion Conference and Exhibit, Sacramento, CA, 2006. AIAA-2006-4485*, 2006.

[13]Foster, J. E. and Patterson, M. J., "Downstream Ion Energy Distributions in a Hollow Cathode Ring Cusp Discharge," *Journal of Propulsion and Power*, Vol. 21, No. 1, Jan. 2005, pp. 144–151.

[14]Gallimore, A. and Rovey, J., "Erosion Processes of the Discharge Cathode Assembly of Ring-Cusp Gridded Ion Thrusters," *Journal of Propulsion and Power*, Vol. 23, No. 6, 2007, pp. 1271–1278.

[15]Goebel, D. M., Jameson, K. K., Katz, I., and Mikellides, I. G., "Potential fluctuations and energetic ion production in hollow cathode discharges," *Physics of Plasmas*, Vol. 14, No. 10, 2007.

[16]Mikellides, I. G., Katz, I., Goebel, D. M., Jameson, K. K., and Polk, J. E., "Wear Mechanisms in Electron Sources for Ion Propulsion, II: Discharge Hollow Cathode," *Journal of Propulsion and Power*, Vol. 24, No. 4, July 2008, pp. 866–879.

[17]Chu, E., Goebel, D. M., and Wirz, R. E., "Reduction of Energetic Ion Production in Hollow Cathodes by External Gas Injection," *Journal of Propulsion and Power*, Vol. 29, No. 5, June 2013, pp. 1155–1163.

[18]Bychenkov, V., Silin, V., and Uryupin, S., "Ion-acoustic turbulence and anomalous transport," *Physics Reports*, Vol. 164, No. 3, 1988, pp. 119 – 215.

[19]de Kluiver, H., Perepelkin, N., and Hirose, A., "Experimental results on current-driven turbulence in plasmas - a survey," *Physics Reports*, Vol. 199, No. 6, 1991, pp. 281 – 381.

[20]Horton, W., *Turbulent Transport in Magnetized Plasmas*, World Scientific, 2012.

[21]Fitzgerald, D., *Plasma Fluctuations in Ion Thrusters Utilizing Hollow Cathodes*, Ph.D Thesis, Colorado State University, 1983.

[22]Farnell, C. and University, C. S., *Plasma Flow Field Measurements Downstream of a Hollow Cathode*, Ph.D Thesis, Colorado State University, 2007.

[23]Sagdeev, R. and Galeev, A., *Nonlinear plasma theory*, Frontiers in physics, W. A. Benjamin, 1969.

[24]Fenneman, D. B., Raether, M., and Yamada, M., "Ion-acoustic instability in the positive column of a helium discharge," *Physics of Fluids*, Vol. 16, No. 6, 1973, pp. 871–878.

[25]Stix, T., *Waves in Plasmas*, AIP, New York, 1992.

[26]Stringer, T., "Low-frequency waves in an unbounded plasma," *Journal of Nuclear Energy. Part C, Plasma Physics, Accelerators, Thermonuclear Research*, Vol. 5, No. 2, 1963, pp. 89.

[27]Kadomtsev, B., *Plasma turbulence*, Academic Press, 1965.

[28]Choi, D.-I. and Wendell Horton, J., "Modified Kadomtsev spectrum from renormalized plasma turbulence theory," *Physics of Fluids*, Vol. 17, No. 11, 1974, pp. 2048–2060.

[29]Honzawa, T. and Kawai, Y., "Ion heating caused by ion acoustic waves in an ion-streaming plasma," *Plasma Physics*, Vol. 14, No. 1, 1972, pp. 27.

[30]Chu, E. and Goebel, D. M., "High-Current Lanthanum Hexaboride Hollow Cathode for 10-to-50-kW Hall Thrusters," *Plasma Science, IEEE Transactions on*, Vol. 40, No. 9, 2012, pp. 2133–2144.

[31]Chen, F. F., "Langmuir probe diagnostics," *Mini-Course on Plasma Diagnostics, IEEE-ICOPS Meeting, Jeju, Korea*, 2003.

[32]Hutchinson, I., *Principles of Plasma Diagnostics*, Cambridge University Press, 2005.

[33]Beall, J. M., Kim, Y. C., and Powers, E. J., "Estimation of wavenumber and frequency spectra using fixed probe pairs," *Journal of Applied Physics*, Vol. 53, No. 6, 1982, pp. 3933–3940.

[34]Williams, G.J., J., Smith, T., Domonkos, M., Gallimore, A., and Drake, R., "Laser-induced fluorescence characterization of ions emitted from hollow cathodes," *Plasma Science, IEEE Transactions on*, Vol. 28, No. 5, 2000, pp. 1664–1675.

[35]Mikellides, I. G., Goebel, D. M., Jorns, B. A., Polk, J., and Guerrero, P., "Numerical Simulation of the Partially-ionized Gas in a 100-A LaB6 Hollow Cathode," *33rd International Electric Propulsion Conference, The George Washington University, Washington, D.C. October 6 10, 2013. IEPC-2007-124*, 2013.

[36]Kawai, Y., Hollenstein, C., and Guyot, M., "Ion acoustic turbulence in a large-volume plasma," *Physics of Fluids*, Vol. 21, No. 6, 1978, pp. 970–974.